J|A|C|S
COMMUNICATIONS

Published on Web 09/18/2004

Structures and Dynamics of Self-Assembled Surface Monolayers Observed by Ultrafast Electron Crystallography

Chong-Yu Ruan, Ding-Shyue Yang, and Ahmed H. Zewail*

Laboratory for Molecular Sciences, Arthur Amos Noyes Laboratory of Chemical Physics, California Institute of Technology, Pasadena, California 91125

Received July 29, 2004; E-mail: zewail@caltech.edu

When a beam of ultrashort electron pulses impinges on a crystal surface, diffraction patterns can be resolved in time (fs to ps) and in space (pm). Because of the large cross-section for electron interaction with matter, the sensitivity is submonolayer. This methodology of ultrafast electron crystallography (UEC)[1−3] makes possible the study of surface atoms[4] and adsorbates of nanometer length scale.[5] In this communication, we report our first study of self-assembled[6] adsorbates on metal surfaces. Specifically, we studied single-crystal clean surfaces of Au(111) with and without a monolayer of reaction involving the assembly of 2-mercaptoacetic acid from 2,2′-dithiodiacetic acid.[7] We also studied monolayers of iron hemes. With UEC, we are able to observe and isolate structural dynamics of the substrate (gold) and adsorbate(s) following an ultrafast temperature jump.

The single-crystal substrate has a long-range order, and this results in well-defined Bragg diffraction spots and streaks in the Laue zones. In the presence of adsorbates, new diffraction features appear depending on the degree of order: Bragg spots if perfectly ordered and Debye−Scherrer rings if ordered but disoriented. Using the method of diffraction frame referencing,[8] gating of the distinct coherent diffraction features (Bragg spots, streaks, or Debye−Scherrer rings), or the incoherent features (diffusive background or Kikuchi scattering) as a function of time allows for independent isolation of dynamics originated from different structures. This isolation is aided by the ability to obtain the diffraction at small and large angles in real time. UEC is thus uniquely suited for examining structural dynamics with atomic-scale spatial and temporal resolutions.

Gold (111) films of 150 nm thickness on mica substrates were purchased from Molecular Imaging; the single-crystal domain from STM images is more than 200 × 200 nm. The thiolated surface was prepared following procedures of ref 7, which we also used for thiolated alkanes and heme assembly. In solution, the disulfide bond of 2,2′-dithiodiacetic acid breaks to form the more stable sulfur−gold interfacial bonds.[7,9] The samples were then rinsed copiously with ethanol, dried in nitrogen ambient, and immediately mounted onto the goniometer of our UEC diffraction UHV chamber (∼5 × 10^{-10} Torr). The apparatus (Figure 1) consists of three chambers (for diffraction, load lock, and sample preparation) and a laser system for the generation of the ultrashort light pulses, one for heating and another for electron diffraction. The goniometer allows for the change of crystal position (three translations) and orientation (two rotations). To initiate the change, we used near-IR 800 nm fs heating pulses,[4] and to probe, we generated ultrashort electron pulses (30 keV). The pulses can be as short as 300−600 fs, but here we used ∼1 ps pulse duration at the number of electrons used; for more details, see refs 2−4 and 8. Care was taken to ensure overlap of the electron and heating pulses.[4] The electron pulses were timed to arrive either before or after the initiating pulse, and diffraction patterns were recorded on a CCD camera assembly

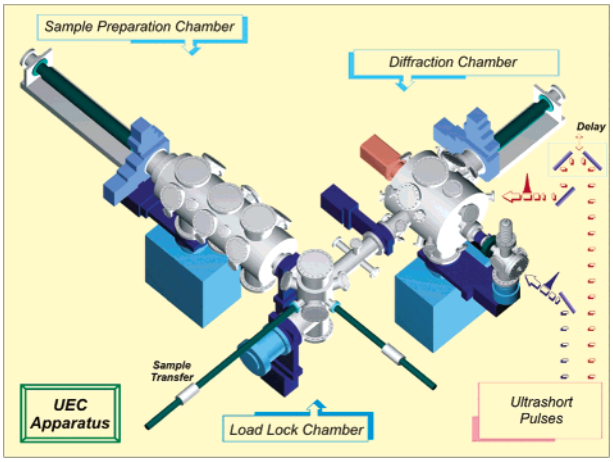

Figure 1. UEC apparatus.

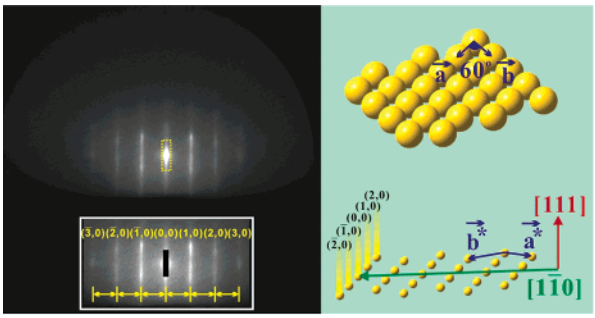

Figure 2. Left: Diffraction images of single-crystal Au(111). The inset shows the streaks at higher contrast, indexed according to the Miller indices (*h*,*k*), where *k* represents the order of Laue zones (see text). Right: Real-space representation of Au(111) (top) together with reciprocal lattice rods corresponding to the two-dimensional Au(111) surface (bottom).

capable of detecting single-electron events. All experiments were performed at room temperature except for studies of diffusive scattering at small angles when we reduced the substrate temperature to 120 K to suppress thermal background.

For the clean unmodified gold substrate, the diffraction patterns consist of well-resolved Bragg spots and streak features (Figure 2). The positions of these spots and streaks, together with the geometrically established specular reflection and shadow edges for calibration, directly provide the structure of the two-dimensional reciprocal lattice of the (111) planes of the face-centered-cubic crystal. As noted in Figure 2, we observed the streaks in the zeroth-order Laue zone, indexed by (*h*,0), where the integer *h* is a Miller index. The rods of the two-dimensional reciprocal lattice are modulated because of the few surface layers in the c* direction of the reciprocal space. We obtained the lattice spacing of the Au-(111) plane, which is consistent with that of the literature X-ray value (d_{Au-Au} = 2.884 Å). We also obtained the rocking curves

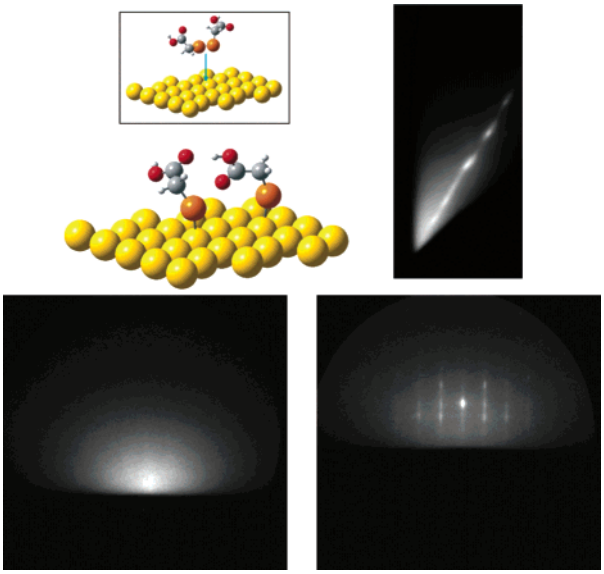

Figure 3. Top left: Representation of the structures involved in the reaction of 2,2′-dithiodiacetic acid and a clean gold surface. Top right: The experimentally observed rocking curve s (vertical) vs θ_{in} (horizontal), where s is the scattering vector and θ_{in} is the incidence angle. Note the different orders observed as a function of θ_{in}, which were detected by gating the (0,0) streak. Bottom left: Static diffuse scattering obtained without time resolution at a small incidence angle of ∼1°. Bottom right: Gold-type streaks (see Figure 2) obtained for the thiolated surface when the incidence angle is relatively large (∼4.2°). Note that the shadow edge is different for small- and large-angle diffractions, reflecting the geometry of electron incidence on the surface.

and observed the different orders satisfying the Bragg/Laue conditions: $sd_{(111)} = 2\pi n$, where n is the order of diffraction and s is the scattering vector, $s = (4\pi/\lambda)\sin(\theta/2)$, with θ being the angle between the incident and outgoing wave vectors and λ the wavelength of the electron (at 30 keV, $\lambda \cong 0.07$ Å). From the rocking curves, the (c*) interplanar Bragg reflections for clean and thiolated gold surfaces were identified at incidence angles of 3.4 and 4.2°, and these Bragg spots were gated to give lattice dynamics of the (111) planes at $d_{(111)} = 2.355$ Å.

The self-assembled monolayer (SAM) on gold results in a much different diffraction pattern, depending on the angle of incidence (Figure 3). At low incidence angles (∼1°), diffuse scattering was observed (Figure 3, bottom left), while at relatively higher incidence angles (∼4.2°), we basically recover the gold-type behavior of Figure 2 (see Figure 3, bottom right). Accordingly, the SAM reaction shown in Figure 3 for 2-mercaptoacetic acid on gold resulted in surface diffraction of what appears to be a randomly oriented adsorbate; however, when the electron was allowed (at the larger incidence angles) to penetrate the bulk surface layers, we recovered gold diffraction even with the thiolated surface layer being present. To check for the order of diffraction, we compared rocking curves with and without thiolation (see Figure 3, top right). This *static* picture was completely altered when we obtained the dynamics using ultrafast initiation by a heating pulse.

Following the ultrafast temperature jump, the structural evolution from Bragg spots was monitored[4] in terms of peak position (lattice expansion), width (integrity of long-range order), and intensity (temperature). Clean and thiolated surfaces show striking differences in structural dynamics (Figure 4). As manifested in the shift of the Bragg spot position on the CCD, the thiolated surface needs only ∼20 ps to reach 80% of its maximum change. This change corresponds to a lattice expansion of 2.2%, or a 52 mÅ increase in the (111) interplanar distance. For the clean gold surface, however, it requires at least ∼55 ps to reach 80%, depending on cleanliness,

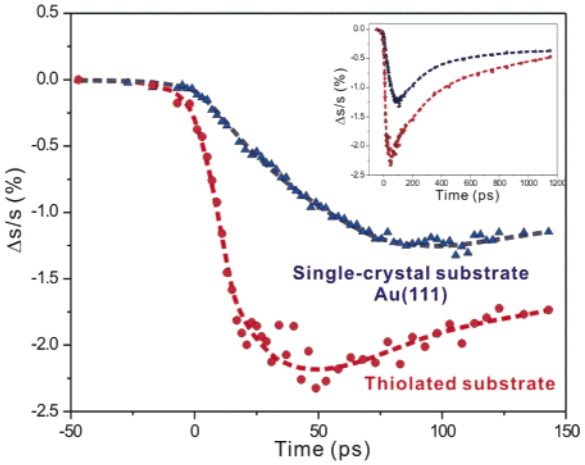

Figure 4. Relative changes of the scattering vector s vs time. The inset shows the restructuring at a much longer time.

of its maximum change (1.3%). The determined surface movement on the order of 0.1 Å is the precursor impulse for adsorbate and bulk lattice heating.

We have observed that the degree of cleanliness and/or surface reconstruction changes the time response; e.g., freshly prepared gold samples give an even slower response. However, the distinct difference between unthiolated and thiolated surfaces is reproducible. It should be noted that the influence of electrons on the surface is inert, as the surface is observed to restructure back to the same ground state (Figure 4, inset), i.e., there is no observed irreversible loss of structure. The evolution of width of the Bragg spot, which reflects the long-range order of the structure along the (111) planes (probed by electrons), is also noticeable: the thiolated surface shows initial broadening (loss of order) followed by narrowing of the peak (enhancement of order), while the clean gold surface shows a slower response. The decrease in peak intensity reflects change in temperature, and again for the thiolated surface, the behavior is different from that of clean gold.

At an incidence angle of ∼1°, i.e., gating the molecular diffraction region, we observed the emergence of Debye−Scherrer rings and the dramatic change in the diffraction background, but only after the IR laser heating (Figure 5). In the radially averaged one-dimensional diffraction intensity curves, these changes in structural dynamics of the adsorbates were followed by monitoring the evolution of diffraction peaks and background. The near maximum formation of the long-range order is reached at 49 ps, as observed in the prominence of the coherent diffraction peaks (Figure 5, bottom). For the incoherent scattering background, an ultrafast increase of intensity (∼5 ps) just after the laser heating is noted and followed by a depletion of intensity for ∼30 ps; at longer times the background continues to increase (Figure 5, bottom). Remarkably, these difference frames are showing the *depletion* (negative difference) at early times and simultaneously the appearance of a coherent ring structure, while at longer times the diffuse signal is positively *increasing* at the expense of the coherent signal. The restructuring is not complete even at 1 ns. As noted in the inset of Figure 4, at ∼1 ns there still remains expansion of the lattice, and similarly here the adsorbate has not fully relaxed and mostly disordered. Ultimately, the frame difference of −17 ps would be recovered, as evidenced from the decrease in scattering amplitude between the frames at long times; see, e.g., $t = 103$ and 1153 ps (Figure 5).

These observations are rich for deciphering structural dynamics of the substrate and adsorbate. First, the observed lattice dynamics of clean gold substrate is unexpected. Although electron−phonon

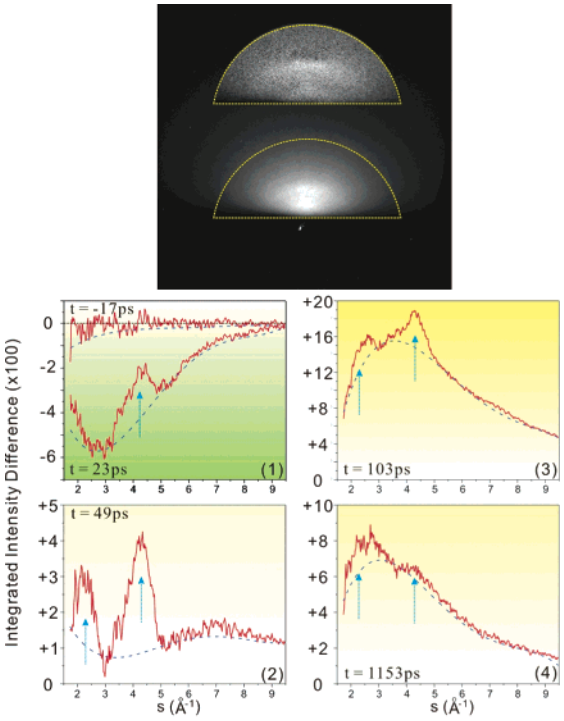

Figure 5. Top: Diffraction image difference following ultrafast heating of the thiolated substrates: $t = 88$ ps; reference $t = -47$ ps (upper). The lower diffraction pattern is a frame at $t = -47$ ps. Bottom: Integrated difference of the radial average versus s at different delay times ($t_{ref} = -47$ ps). Frames 1−4 describe the following: (1) reference to negative time (−47 ps) frame at −17 ps and depletion of diffuse scattering at $t = 23$ ps; (2) coherent diffraction; (3) increase of diffuse scattering; and (4) recovery of diffuse scattering. Dashed lines represent simulated (polynomial) incoherent scattering and upward arrows indicate the positions of coherent peaks. Note the positive and negative change in the difference and the different scales used on the vertical axes.

coupling is known in metallic gold to occur within ~1 ps,[10] the observed increase in lattice expansion in nearly 50 ps (instead of a decrease after ~1 ps) elucidates the existence of a nonequilibrium state among the modes responsible for surface and lattice expansion. Since our electron probing region is within the optically heated depth (~13 nm; skin depth $= \lambda/4\pi k$, with the imaginary part of refractive index k being ~5 at $\lambda = 800$ nm[11]), complete equilibration will not lead to further expansion after 1 ps. Accordingly, the observed changes are due to the slower coupling between high-frequency (local) modes excited at an early time and the lattice acoustic (coherent and long-range) modes that lead to the expansion; at longer times the system equilibrates and the lattice restructures, as shown in Figure 4. Because of the mismatch between mode frequencies, this behavior is reminiscent of energy redistribution in molecules,[12] and the time constant is not significantly different from those of semiconductors (~30 ps for Si,[1] and ~12 ps for GaAs[4]). The change in expansion dynamics from the unmodified gold surface to the thiolated surface is thus consistent with the adsorbate having many modes: energy can flow more effectively to them than to the mismatched low-frequency acoustic modes of bulk lattice.

The diffraction pattern at small angle and negative time, i.e., when the electron pulse diffracts before the arrival of the heating pulse, appears to be diffusive. However, as shown in Figure 5, the coherent scattering (Debye−Scherrer rings) becomes dominant at a positive time of 49 ps. Thus, the timing of the electron pulse is critical for structural isolation and determination. Because the s value below the shadow edge is ≤ 1.5 Å^{-1} at our incidence angle and camera length, the coherent peak positions are of $n = 2$ and 3. From the corresponding s values, we obtained a lattice constant of 5 ± 0.6 Å for the molecular assembly. This distance is reasonable given that typical S−S distance is $\sim\sqrt{3}$ times the Au−Au distance (2.884 Å), i.e., ~5 Å.[13]

Dynamically speaking, this temporally isolated coherent diffraction from the assembly reaches its maximum but then is lost to the incoherent background at longer times, indicating that the orientational order of the assembly is dynamically controlled, and we can establish the time scale for this "ultrafast annealing." The evolution of background scattering also reflects the change in the long-range surface order and homogeneity. The initial temperature jump introduces dramatic depletion of the background within the first ~30 ps, and then a swift inversion of the trend appears, during which the molecular coherent peak sharpens and the background scattering begins to increase significantly. The initial depletion reflects the transient temperature-induced homogeneity, while after 30 ps the identity of inhomogeneous surface distributions leads to the increase of the background intensity (Figure 5). Clearly, the time resolution is essential for isolating coherent structural dynamics of the self-assembled layers, which statistically are not ordered at long times!

We have demonstrated that the structure and dynamics of self-assembled monolayer and metal substrate can be isolated and studied with unprecedented spatial and temporal resolutions and with monolayer sensitivity. This is made possible using UEC and its ability to isolate diffraction at different angles of real-time frames with atomic-scale resolution. Moreover, it is shown that for complex molecular structures, the resolution in time is crucial for observing the coherent diffraction (ordered structure), otherwise buried in diffusive scattering (disordered structure), and at long times disorder of assembly is evident. With this in mind, we also studied monolayers of alkanethiols and thio-derivatized hemes on Au(111) surfaces, and were able to record the diffraction; the more refined structural dynamics will be published later. Currently, we are extending the applications to SAMs of longer chains and biological networks.

Acknowledgment. This work was supported by the National Science Foundation. We thank Dr. J. K. Amisha Kamal for the preparation of the samples.

References

(1) Thomas, J. M. *Angew. Chem., Int. Ed.* **2004**, *43*, 2606.
(2) Ruan, C.-Y.; Vigliotti, F.; Lobastov, V. A.; Chen, S.; Zewail, A. H. *Proc. Natl. Acad. Sci. U.S.A.* **2004**, *101*, 1123.
(3) Lobastov, V. A.; Srinivasan, R.; Vigliotti, F.; Ruan, C.-Y.; Feenstra, J.; Chen, S.; Park, S. T.; Xu, S.; Zewail, A. H. In *Ultrafast Optics IV*; Springer Series in Optical Sciences; Krausz, F., Korn, G., Corkum, P., Walmsley, I., Eds.; Springer-Verlag: Berlin, 2003; p 413.
(4) Vigliotti, F.; Chen, S.; Ruan, C.-Y.; Lobastov, V. A.; Zewail, A. H. *Angew. Chem., Int. Ed.* **2004**, *43*, 2705.
(5) Ruan, C.-Y.; Lobastov, V. A.; Vigliotti, F.; Chen, S.; Zewail, A. H. *Science* **2004**, *304*, 5667.
(6) Bain, C. D.; Whitesides, G. M. *Science* **1988**, *240*, 62 and references cited therein.
(7) Shimizu, M.; Kobayashi, K.; Morii, H.; Mitsui, K.; Knoll, W.; Nagamune, T. *Biochem. Biophys. Res. Commun.* **2003**, *310*, 606 and references cited therein.
(8) Srinivasan, R.; Lobastov, V. A.; Ruan, C.-Y.; Zewail, A. H. *Helv. Chim. Acta* **2003**, *86*, 1761 and references cited therein.
(9) Nuzzo, R. G.; Allara, D. L. *J. Am. Chem. Soc.* **1983**, *105*, 4481.
(10) (a) Sun, C.-K.; Vallée, F.; Acioli, L. H.; Ippen, E. P.; Fujimoto, J. G. *Phys. Rev. B* **1994**, *50*, 15337 and references cited therein. (b) Suárez, C.; Bron, W. E.; Juhasz T. *Phys. Rev. Lett.* **1995**, *75*, 4536 and references cited therein.
(11) Johnson, P. B.; Christy, R. W. *Phys. Rev. B* **1972**, *6*, 4370.
(12) Felker, P. M.; Zewail, A. H. *Phys. Rev. Lett.* **1984**, *53*, 501.
(13) Ulman, A. *Chem. Rev.* **1996**, *96*, 1533.

JA045441N